THE ROYAL SOCIETY

Acoustic cavitation and its chemical consequences

By Kenneth S. Suslick, Yuri Didenko, Ming M. Fang, Taeghwan Hyeon, Kenneth J. Kolbeck, William B. McNamara III, Millan M. Mdleleni and Mike Wong

School of Chemical Sciences, University of Illinois at Urbana-Champaign, 600 S. Mathews Ave., Urbana, IL 61801, USA

Acoustic cavitation is responsible for both sonochemistry and sonoluminescence. Bubble collapse in liquids results in an enormous concentration of energy from the conversion of the kinetic energy of liquid motion into heating of the contents of the bubble. The high local temperatures and pressures, combined with extraordinarily rapid cooling, provide a unique means for driving chemical reactions under extreme conditions. A diverse set of applications of ultrasound to enhance chemical reactivity has been explored, with important applications in mixed-phase synthesis, materials chemistry, and biomedical uses. For example, the sonochemical decomposition of volatile organometallic precursors in low-volatility solvents produces nanostructured materials in various forms with high catalytic activities. Nanostructured metals, alloys, carbides and sulphides, nanometre colloids, and nanostructured supported catalysts can all be prepared by this general route. Another important application of sonochemistry to materials chemistry has been the preparation of biomaterials, most notably protein microspheres. Such microspheres have a wide range of biomedical applications, including their use as echo contrast agents for sonography, magnetic resonance imaging contrast enhancement, and oxygen or drug delivery.

Keywords: sonochemistry; sonoluminescence; materials; nanostructures; microspheres

1. Introduction

The chemical effects of ultrasound (Suslick 1988, 1998; Mason & Lorimer 1988) do not derive from a direct coupling of the acoustic field with chemical species on a molecular level. Instead, sonochemistry and sonoluminescence derive principally from acoustic cavitation: the formation, growth and implosive collapse of bubbles in liquids irradiated with high-intensity ultrasound (Leighton 1994). Bubble collapse during cavitation serves as an effective means of concentrating the diffuse energy of sound: compression of a gas generates heat. When the compression of bubbles occurs during cavitation, heating is more rapid than thermal transport, creating a short-lived localized hot spot. There is a nearly universal consensus that this hot spot is the source of homogeneous sonochemistry. Rayleigh's early descriptions of a mathematical model for the collapse of cavities in incompressible liquids predicted enormous local temperatures and pressures (Rayleigh 1917). Ten years later, Richards & Loomis (1927) reported the first chemical effects of ultrasound. Cavitation was heavily studied during the 1950s and 1960s, culminating in a relatively detailed

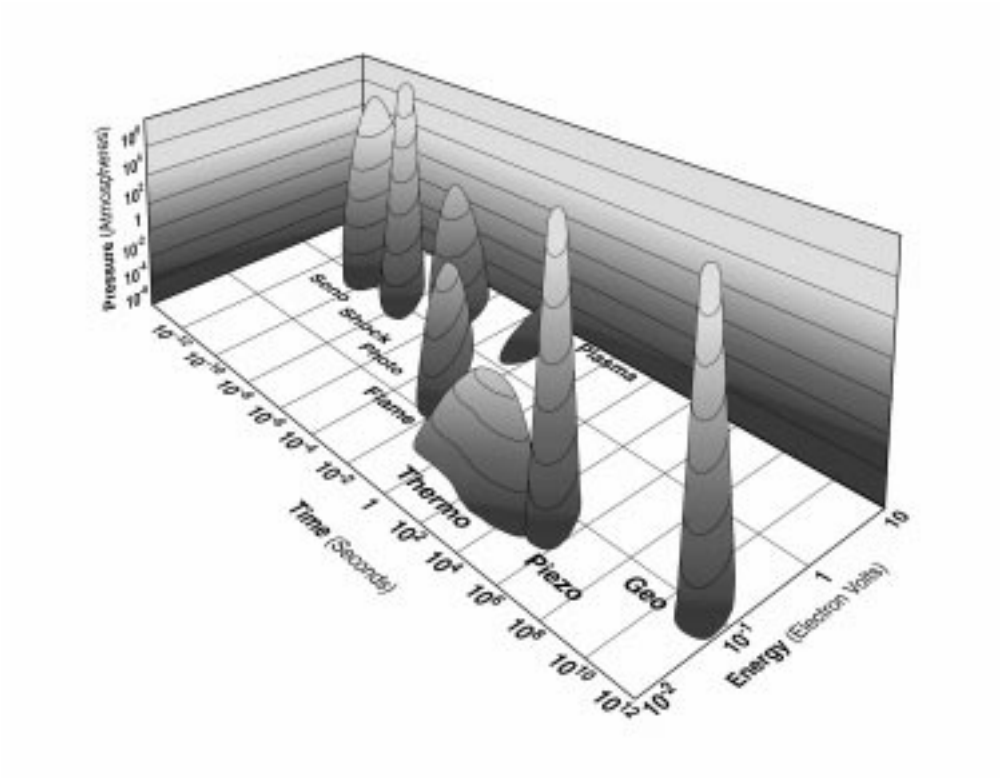

Figure 1. Chemistry: the interaction of energy and matter.

understanding (Neppiras 1980; Flynn 1964). From that time on, the chemical effects of ultrasound have been well explained as the consequence of localized hot spots created during bubble collapse.

Emission of light often accompanies sonochemistry. Such sonoluminescence provides an extremely useful spectroscopic probe of the conditions created during cavitation bubble collapse (Suslick 1990; Suslick & Crum 1997). As with sonochemistry, sonoluminescence is a consequence of acoustic cavitation. The collapse of bubbles caused by cavitation produces intense local heating and high pressures, with very short lifetimes. As we will show in this paper, the collapse of bubbles in a multibubble cavitation field produces hot spots with effective temperatures of *ca.* 5000 K, pressures of *ca.* 1000 atm, and heating and cooling rates above 10^{10} K s^{-1}. In single-bubble cavitation, conditions may be even more extreme (Crum 1994*a*; Putterman 1995). Thus, cavitation can create extraordinary physical and chemical conditions in otherwise cold liquids.

Chemistry is fundamentally the interaction of energy and matter. Chemical reactions require energy in one form or another to proceed: chemistry stops as the temperature approaches absolute zero. Chemists have only limited control, however, over the nature of this interaction. In large part, the properties of a specific energy source determine the course of a chemical reaction. Ultrasonic irradiation differs from traditional energy sources (such as heat, light or ionizing radiation) in duration, pressure and energy per molecule. The immense local temperatures and pressures together

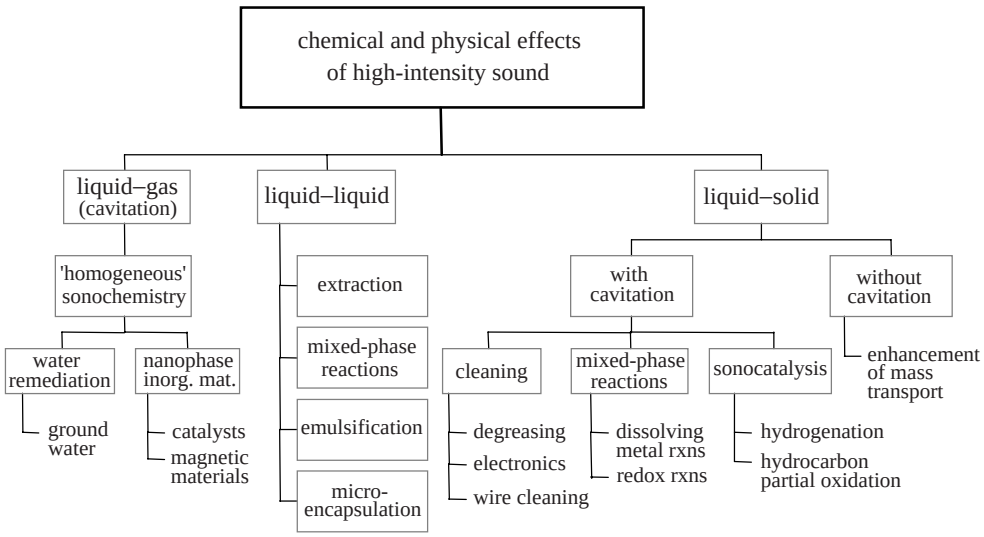

Figure 2. Classification of the chemical and physical effects of ultrasound.

with the extraordinary heating *and* cooling rates generated by cavitation bubble collapse mean that ultrasound provides a unique mechanism for generating high-energy chemistry. Figure 1 presents an interesting comparison of the parameters that control chemical reactivity (time, pressure and energy) for various forms of chemistry.

There is a wide range of chemical and physical consequences that high intensity can induce, as shown schematically in figure 2. The chemical effects of ultrasound can be divided into three general types: neat liquids; heterogeneous liquid–liquid; and heterogeneous liquid–solid systems. Sonocatalysis, i.e. the use of ultrasound to initiate or modify catalytic reactions, overlaps these classes. Over the past few years, the synthesis of inorganic and bio-materials has developed as one of the most important applications of sonochemistry (Suslick 1995, 1997). Cavitation provides a unique set of conditions to produce unusual materials from precursors dissolved in solution. In order to illustrate the utility of ultrasound in the synthesis of new and unusual materials, we will examine several recent examples discovered at the University of Illinois. Specifically, the sonochemical synthesis of nanostructured amorphous metals and alloys, nanocolloids of Fe, and nanostructured MoS_2 will be described.

Although length limitations prevent a detailed discussion here, the role of ultrasound in increasing reactivity in liquid–solid systems has proved extremely important in chemical synthesis (Suslick 1994; Mason & Luche 1996). Cavitation has dramatic effects on the reactivities of solutions containing either extended solid surfaces or fine powders. Cavity collapse near an extended solid surface becomes non-spherical, drives high-speed jets of liquid into the surface, and creates shockwave damage to the surface (Leighton 1994). This process can produce newly exposed highly heated surfaces and is responsible for the erosion/corrosion problems associated with hydrodynamic cavitation (Preece & Hansson 1981). Furthermore, cavitation and the shockwaves produced during ultrasonic irradiation of liquid–powder slurries can accelerate solid particles to high velocities (Suslick & Doktycz 1990; Doktycz & Suslick 1990). The interparticle collisions that result are capable of inducing striking changes in surface morphology, composition and reactivity. Thus, microjet and shockwave impact (on

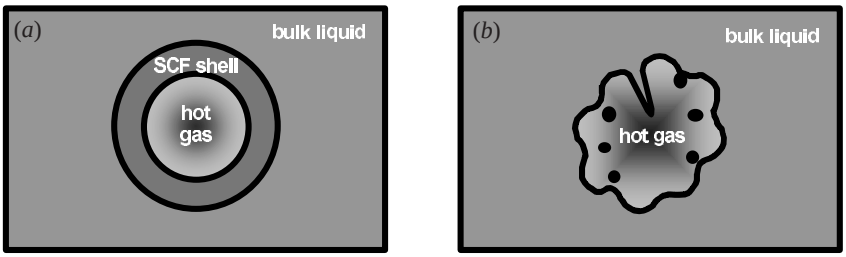

Figure 3. Two-site models of sonochemical reactions. (*a*) Thermal diffusion shell model; (*b*) surface wave droplet and jet model.

large surfaces) and interparticle collisions (with powders) have substantial effects on the chemical composition and physical morphology of solids that can dramatically enhance chemical reactivity.

2. Two-site model of sonochemical reactivity

The transient nature of cavitation, especially in bubble clouds, precludes conventional measurement of the conditions generated during bubble collapse. Chemical reactions themselves, however, can be used to probe reaction conditions. The effective temperature realized by the collapse of bubbles in cavitation clouds can be determined by the use of competing unimolecular reactions whose rate dependencies on temperature have already been measured. This technique of 'comparative-rate chemical thermometry' was used by Suslick *et al*. (1986) to make the first experimental determination of the effective temperature reached during cavity collapse. The sonochemical ligand substitutions of volatile metal carbonyls were used as the comparative rate probes. These kinetic studies revealed that there are in fact *two* sonochemical reaction sites: the first (and dominant site) is the bubble's interior gas-phase, while the second is an *initially* liquid phase. The latter corresponds either to the heating of a shell of liquid around the collapsing bubble or to the injection of liquid droplets into the hot spot by surface-wave distortions or jets of the collapsing bubble, as shown schematically in figure 3.

The effective local temperatures in both sites were determined by combining the relative sonochemical reaction rates for ligand dissociation with the known temperature behaviour of these reactions. The effective temperatures of these hot spots were measured at *ca.* 5200 K in the gas-phase reaction zone and *ca.* 1900 K in the initially liquid zone (Suslick *et al*. 1986). Of course, the comparative rate data represent only a composite temperature: during the collapse, the temperature within the bubble has a rapidly changing temporal and spatial profile. This two-site model has been confirmed with other reactions (Henglein 1993). The study of sonoluminescence, which will now be discussed, has both confirmed and extended these temperature measurements of the cavitation hot spot.

3. Sonoluminescence

(*a*) *Types of sonoluminescence*

Sonoluminescence was first observed from water by Frenzel & Schultes (1934). As with sonochemistry, sonoluminescence derives from acoustic cavitation. There are

two classes of sonoluminescence (Crum 1994*a*, *b*; Matula *et al*. 1995): multiple-bubble sonoluminescence (MBSL) and single-bubble sonoluminescence (SBSL). Cavitation is a nucleated process and liquids generally contain large numbers of particulates that serve as nuclei. Consequently, the 'cavitation field' generated by a propagating or standing acoustic wave typically consists of very large numbers of interacting bubbles distributed over an extended region of the liquid. If this cavitation is sufficiently intense to produce sonoluminescence, then this phenomenon is called 'multiple-bubble sonoluminescence'.

Under appropriate conditions, the acoustic force on a bubble can balance against its buoyancy, holding the bubble stable in the liquid by acoustic levitation. This permits examination of the dynamic characteristics of the bubble in considerable detail, from both a theoretical and an experimental perspective. Such a bubble is typically quite small compared to an acoustic wavelength (e.g. at 20 kHz, the maximum radius observed during SBSL is *ca*. 50 μm). It was recently discovered, for rather specialized but easily obtainable conditions, that a single stable oscillating gas bubble can be forced into such large-amplitude pulsations that it produces sonoluminescence emissions during each (and every) acoustic cycle (Cheeke 1997; Barber *et al*. 1997). This phenomenon is called 'single-bubble sonoluminescence'.

(*b*) *MBSL spectra*

Over the last three decades, the sonoluminescence of aqueous solutions has been studied at length, most recently and carefully by Didenko and co-workers (Didenko *et al*. 1994; Didenko & Pugach 1994). The spectrum of MBSL in water consists of a peak at 310 nm and a broad continuum spanning the visible region. The emission at 310 nm is from excited-state $OH^{\bullet}$, but the continuum is difficult to interpret. MBSL spectra from aqueous and alcohol solutions of many metal salts have been reported and are characterized by emission from metal-atom excited states (Flint & Suslick 1991*a*).

Sonoluminescence spectra have also been examined for non-aqueous liquids. Flint & Suslick (1989) reported the first MBSL spectra of organic liquids and found that the spectra were consistent with thermal excitation rather than electrical discharge. The observed emission during ultrasonic irradiation of various hydrocarbons comes from excited states of C_2 ($d^3\Pi_g$–$a^3\Pi_u$, the Swan lines), the same emission that is seen in flames. Furthermore, the ultrasonic irradiation of hydrocarbons in the presence of N_2, NH_3 or amines gives emission from CN excited states, but not from N_2 excited states. Emission from N_2 excited states would have been expected if the MBSL originated from microdischarge, whereas CN emission is typically observed from thermal sources. When oxygen is present, emission from excited states of CO_2, $CH^{\bullet}$ and $OH^{\bullet}$ is observed, again similar to flame emission.

Most recently, we have extended our spectral analysis approach to excited-metal-atom MBSL spectra. Ultrasonic irradiation of volatile organometallics ($Fe(CO)_5$ or $Cr(CO)_6$, for example) in a low-volatility organic liquid produces intense sonoluminescence that corresponds to the known atomic emission lines of the metals (Suslick *et al*. 1993), again analogous to flame emission. Hot-spot temperatures are sufficient not only to dissociate all the CO ligands from the metal complex, but also to produce excited-state metal atoms. Figure 4 shows a typical MBSL spectrum from a metal carbonyl solution ($Cr(CO)_6$ in this example). Note the intense line emission from

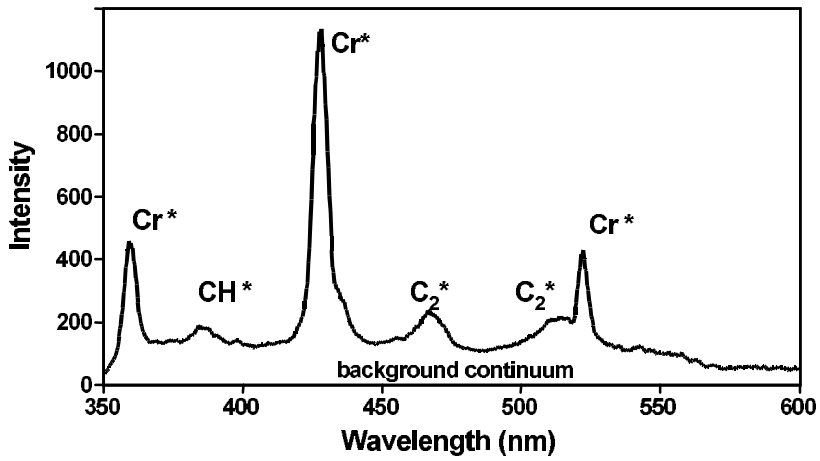

Figure 4. Typical MBSL spectrum from a metal carbonyl solution in silicone oil.

the metal-atom excited states as well as bands from excited states of the diatomics, C_2 and CH.

For both aqueous and non-aqueous liquids, MBSL is caused by chemical reactions of high-energy species formed during cavitation by bubble collapse. Its principal source is most probably not blackbody radiation or electrical discharge. MBSL is a form of chemiluminescence, not unlike flame emission.

(*c*) *The sonoluminescence spectrum as a probe cavitation condition*

Determination of the conditions reached in a cavitating bubble has remained a difficult experimental problem. Spectral analysis of MBSL provides a solution. We have used two very different spectroscopic reporters to provide such information:

(i) resolved molecular emission from diatomics (notably C_2) produced during cavitation; and

(ii) atomic line emission derived from the sonolysis of volatile organometallic compounds.

Flint & Suslick first reported high-resolution MBSL spectra from silicone oil under Ar (Flint & Suslick 1991*b*). The observed emission comes from excited-state C_2 and has been modelled with synthetic spectra as a function of rotational and vibrational temperatures (as shown in figure 5). From comparison of synthetic to observed spectra for several different emission bands, the effective rotational and vibrational emission temperature is 5050 ± 150 K. The excellence of the match between the observed MBSL and the synthetic spectra provides definitive proof that the sonoluminescence event is a thermal chemiluminescence process, although the issue of thermal equilibration in such systems is not without its complexities (Jeffries *et al*. 1992). The agreement between this spectroscopic determination of the cavitation temperature and that made by comparative-rate thermometry of sonochemical reactions (Suslick *et al*. 1986) is surprisingly good.

We have now analysed the relative intensities of atomic emission lines in the sonoluminescence spectra of excited-state metal atoms produced by sonolysis of volatile

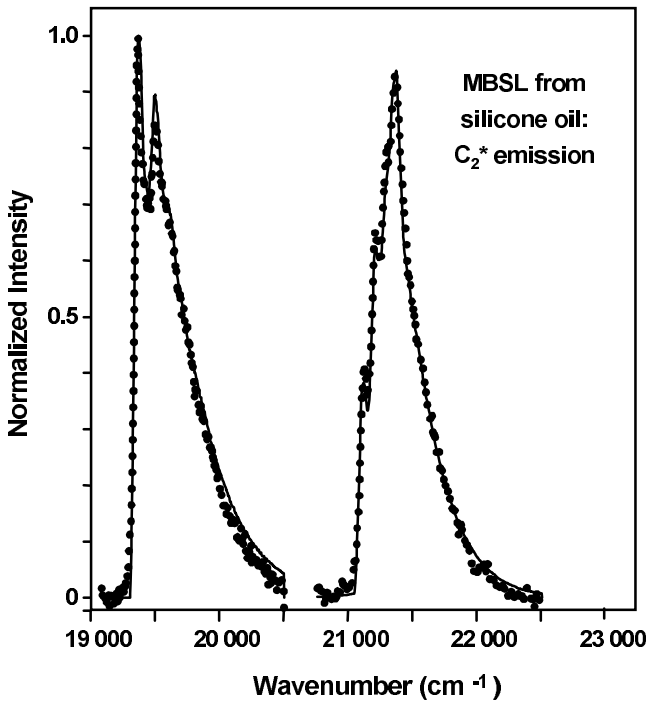

Figure 5. Excited-state C_2 MBSL spectrum from silicone oil under Ar. Emission from the $\Delta v = +1$ manifold of the $d^3\Pi_g$–$a^3\Pi_u$ transition (Swan band) of C_2 (Suslick *et al.* 1986). Observed MBSL spectrum from polydimethylsiloxane oil under Ar at 0 °C (· · · · ·). Best-fit synthetic spectrum for these two bands, with $T_v = T_r = 4900$ K (——).

Fe, Cr and Mo carbonyls dissolved in silicone oil under argon. Sufficient spectral information about emissivities of many metal-atom excited states are available to readily calculate emission spectra as functions of temperature. Because of this, the emission spectra of metal atoms are extensively used to monitor the surface temperature of stars. For example, the expected spectra for iron emission as functions of temperature are shown in figure 6.

From comparison of such calculated spectra and the observed MBSL spectra from metal carbonyls, another measurement of the cavitation temperature can be obtained. The effective emission temperature during cavitation under argon at 20 kHz is 4900 ± 250 K, with excellent agreement among the three systems tested (5150 ± 300 K for Fe, 4700 ± 400 K for Cr and 4750 ± 400 K for Mo), as shown in examples given in figures 7 and 8. Again, agreement with our prior comparative-rate thermometry and the MBSL emission temperature of C_2^* excited states is excellent.

We are also able to control the temperature within the cavitation bubble simply by changing the bubble contents. Upon addition of gaseous hydrocarbons (methane, ethylene or propane), the observed emission temperatures from Cr atom excited states systematically decrease: just 3% propane in Ar, for example, reduces the measured emission temperature to 2500 K. As polyatomic molecules are added to the bubble contents, the polytropic ratio of the gas in the bubble decreases, and so too does the expected temperature from adiabatic compression, as shown by equa-

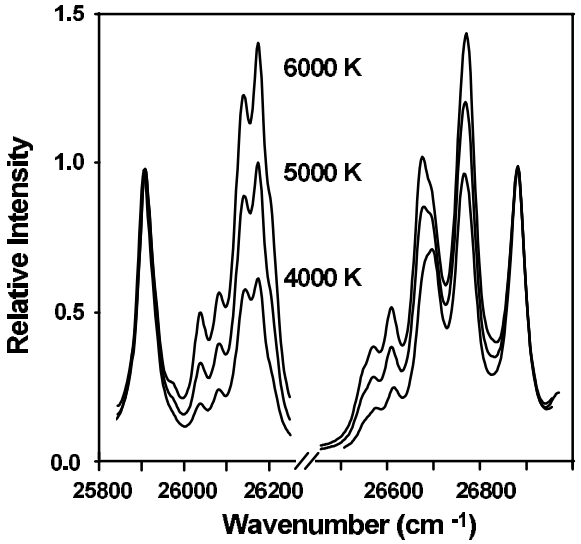

Figure 6. Calculated emission spectra of Fe atoms as functions of temperature.

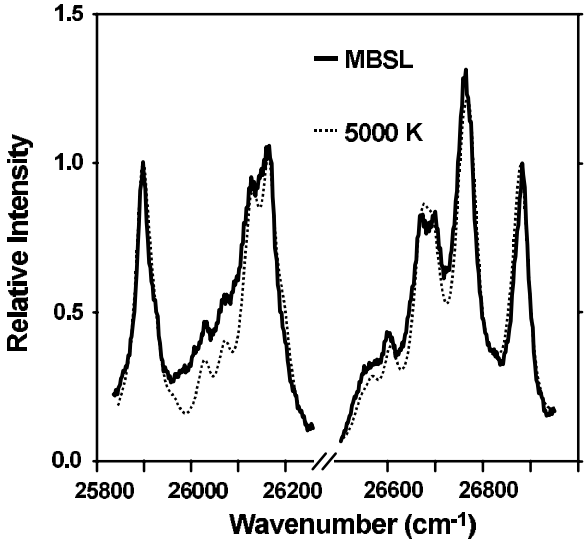

Figure 7. Sonoluminescence of excited-state Fe atoms produced during sonolysis of $Fe(CO)_5$ dissolved in silicone oil under Ar. Effective emission temperature is 5150 ± 300 K.

tion (3.1):

$$T_{\max} = T_{\min}(R_{\max}/R_{\min})^{3(\gamma-1)}. \tag{3.1}$$

The presence of the polyatomic gas simply provides vibrational and rotational modes that will divert much of the kinetic energy of collapse away from a direct temperature increase. The effects of the addition of polyatomic gases on the observed cavitation emission temperature can be quantitatively modelled by simple adiabatic compression of a bubble during cavitational collapse. This simple model predicts

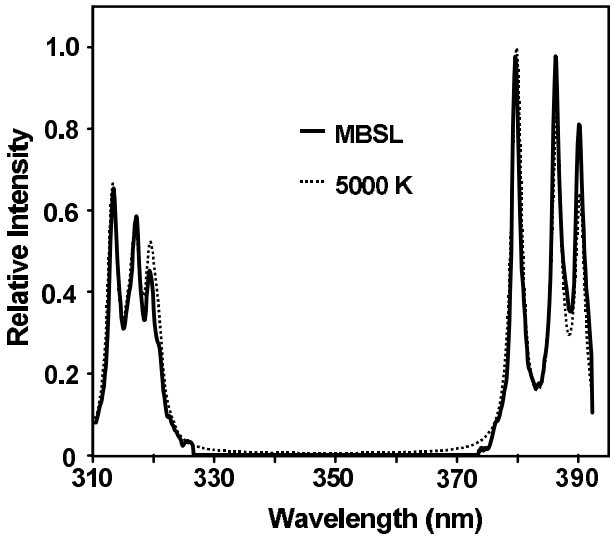

Figure 8. Sonoluminescence of excited-state Mo atoms produced during sonolysis of $Mo(CO)_6$ dissolved in silicone oil under Ar. Effective emission temperature is 4750 ± 400 K.

pressures of the order of 10^3 bar, which is quantitatively consistent with the linewidth broadening and small peak-wavelength shifts observed in the metal-atom emission. The lifetime of the hot spot is less well determined. Certainly, it is under 1 μs and may be considerably less, given the 200 ps emission lifetimes seen in SBSL. The cooling rates, even at microsecond lifetimes, are enormous: above 10^{10} K s^{-1}.

(*d*) *SBSL spectra*

It has recently proved possible to trap a single stable bubble in a standing wave in a spherical or cylindrical transducer. Under certain conditions, a single bubble can be driven sufficiently hard so as to produce sonoluminescence. Study of this SBSL has provided much insight into the physics of cavitation. Unfortunately, single bubbles simply do not contain sufficient material to be useful for driving chemical reactions in any practical amount. In multibubble systems ('cavitation clouds'), on the other hand, the interactions between bubbles as they collapse will lead to both substantial asymmetry and the formation of jets during collapse (Leighton 1994), which one may well expect to limit the collapse efficiency. Thus, the conditions created during multibubble cavitation, which is used of necessity for all sonochemical reactions, will be less extreme than those created during SBSL.

The spectra of MBSL and SBSL are dramatically different (Matula *et al*. 1995), and the interpretation of SBSL spectra is much less clear. MBSL can be observed in essentially all liquids, whereas SBSL has been observed primarily in aqueous liquids. While MBSL is generally dominated by atomic and molecular emission lines (e.g. excited states of $OH^{\bullet}$ in water and of C_2 in hydrocarbons), SBSL is an essentially featureless emission that increases with decreasing wavelength. Unusual effects on the intensity of this featureless SBSL emission are observed when the gas contents of the bubble are changed (Barber *et al*. 1997; Cheeke 1997; Lohse *et al*. 1997; Barber *et al*. 1992). Furthermore, the SBSL spectra show no evidence of OH emission, and when He and Ar bubbles are considered, continue to increase in intensity even into the

deep ultraviolet. For example, the MBSL spectrum of an aqueous solution of NaCl is dominated by strong features from excited states of both $OH^{\bullet}$ and Na; however, the SBSL spectrum of an identical solution shows no evidence of these peaks (Matula *et al*. 1995). Similarly, the MBSL spectrum falls off at low wavelengths, while the SBSL spectrum continues to rise, at least for most noble gases.

Early work on SBSL stirred intense interest due, primarily, to the exceptionally short duration of the sonoluminescence flash. The initial reports by Putterman placed the emission lifetimes well below 50 ps (Barber & Putterman 1992; Barber *et al*. 1997), but more recent studies by Gompf *et al*. (1997) have shown that the emission is generally longer, *ca*. 200 ps, and varies with dissolved-gas concentration and acoustic pressure. Hiller *et al*. (1998) have confirmed these results, but are still able to find lifetimes of *ca*. 50 ps under some conditions. The standard hydrodynamic models of adiabatic collapse of a single bubble could not have explained emission lifetimes much below 50 ps, which generated a wide range of quite speculative theories on the origin of SBSL. The consensus appears to be settling on intense adiabatic compression, leading to the reaction of O_2 and N_2 from air-filled bubbles with rectification into the water of NO_x products (Lohse *et al*. 1997). Partial ionization occurring in the last hottest stages of bubble collapse generate a featureless bremsstrahlung emission (Moss *et al*. 1997; Bernstein *et al*. 1996). There may also be a convergent shockwave within the single bubble (Barber *et al*. 1994), although this remains an open issue.

The difference between SBSL and MBSL spectra appears likely to be related to the severity of collapse. In SBSL, where bubble collapse is more spherical and the extent of compression greater, sufficient temperatures are reached (probably above *ca*. 20 000 K) to form a plasma and the primary emission becomes electron–ion or electron–atom bremsstrahlung (Moss *et al*. 1997; Bernstein *et al*. 1996). In such plasma, the temperatures will ensure dissociation of all molecules and will broaden, through Stark and pressure effects, any remaining molecular or atom emission beyond recognition (Moss *et al*. 1997). The issue of a spherically convergent shockwave and the possibility of extraordinarily high-energy conditions (Moss *et al*. 1997; Barber *et al*. 1994) remains an open question, since direct observation of core conditions will be shielded by the opacity of the surrounding plasma.

4. Synthesis of nanostructured inorganic materials

Solids made from nanometre-sized components often exhibit properties distinct from those of the bulk, in part because clusters that small have electronic structures with a high density of states, but not continuous bands (Weller 1993; Moser 1996). Such nanostructured materials are of intense current interest, and several preparative methods have been developed for their synthesis. Nanostructured-material syntheses include both gas-phase techniques (e.g. molten-metal evaporation, flash-vacuum-thermal and laser-pyrolysis decomposition of volatile organometallics); liquid-phase methods (e.g. reduction of metal halides with various strong reductants, colloid techniques with controlled nucleation); and mixed-phase approaches (e.g. synthesis of conventional heterogeneous catalysts on oxide supports, metal-atom vapour deposition into cryogenic liquids, explosive shock synthesis). Over the past ten years we have added the sonochemical reactions of volatile organometallics to this range of techniques, as a general approach to the synthesis of nanophase materials (figure 9).

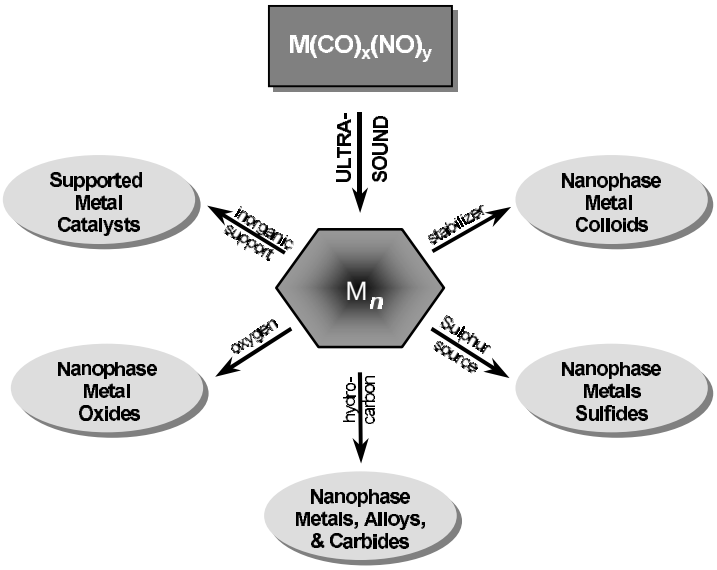

Figure 9. Sonochemical synthesis of nanostructured materials ($n \approx 100$–1000).

We have used the extreme conditions of cavitation to produce a variety of nanostructured and often amorphous metals, alloys and carbides, and have examined their catalytic activity (Suslick 1995, 1997; Suslick *et al*. 1996*b*; Hyeon *et al*. 1996). Volatile organometallic compounds decompose inside a collapsing bubble, and the resulting metal atoms agglomerate to form nanostructured materials. Our sonochemical synthesis of nanostructured materials is also extremely versatile: various forms of nanophase materials can be generated simply by changing the reaction medium (figure 9). When precursors are sonicated in low-volatility alkanes, nanostructured metal powders are formed. If sonication occurs in the presence of a bulky or polymeric surface ligand, stable nanophase metal colloids are created. Sonication of the precursor in the presence of an inorganic support (silica or alumina) provides an alternative means of trapping the nanometre clusters. The nanoparticles, once fixed on the surface of these supports, are very active supported heterogeneous catalysts.

(*a*) *Amorphous metals*

The ultrasonic irradiation of solutions containing volatile transition-metal carbonyls (e.g. $Fe(CO)_5$, $Co(CO)_3NO$) produces highly porous aggregates of nanometre-sized clusters of amorphous metals (Suslick *et al*. 1991; Grinstaff *et al*. 1993; Bellissent *et al*. 1993). For example, sonication of 1 M iron pentacarbonyl in decane at 0 °C under a flow of argon yielded a dull black powder. Elemental analysis of the powder, after heating at 100 °C under vacuum to remove residual solvent, showed it to be greater than 96% iron by weight, with trace amounts of carbon (less than 3%) and oxygen (1%, by difference), presumably from the decomposition of alkane solvent or carbon monoxide during ultrasonic irradiation. Scanning electron micrographs (SEMs) revealed that the powder is an agglomerate of 20 nm particles (figure 10). Transmission electron micrographs (TEMs) further indicated that these 20 nm particles consist of smaller 4–6 nm particles.

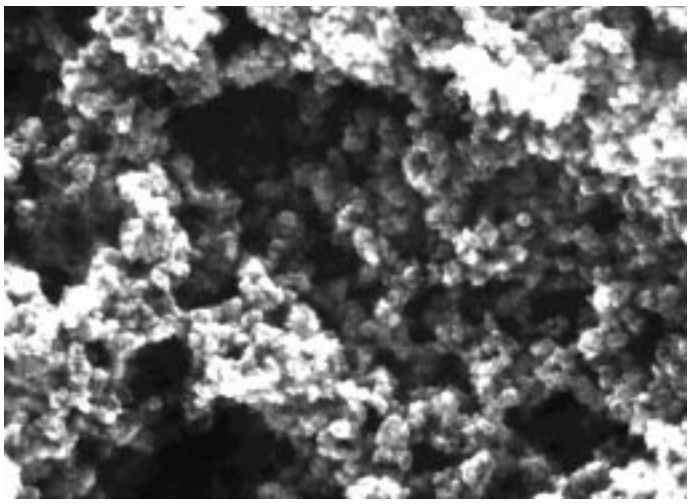

Figure 10. SEM of amorphous iron prepared by the sonochemical decomposition of $Fe(CO)_5$ (Suslick *et al*. 1991). Image size is $1.20 \times 1.67\ \mu m^2$.

The amorphous nature of the iron powder was confirmed by several different techniques, including SEM, differential scanning calorimetry (DSC), electron microdiffraction, X-ray powder diffraction and neutron diffraction. Initial X-ray powder diffraction showed no diffraction peak; after heat treatment under helium at 350 °C the diffraction lines characteristic of BCC iron metal are observed. Electron microdiffraction revealed a diffuse ring pattern, characteristic of amorphous materials. DSC also shows one exothermic irreversible disorder–order transition temperature at 308 °C. The amorphous metal formation appears to result from the extremely high cooling rate during acoustic cavitation.

There had been a long-standing controversy concerning the magnetic properties of amorphous iron, which had not been previously available without a substantial amount of added alloying elements (e.g. boron). Magnetic studies of the sonochemically prepared amorphous iron showed that amorphous iron is a very soft ferromagnetic with a saturation magnetization of *ca*. 173 emu g^{-1} and a Curie temperature in excess of 580 K. The effective magnetic moment is $1.7\mu_B$ with an effective exchange constant of only *ca*. 30% of crystalline Fe (Grinstaff *et al*. 1993; Bellissent *et al*. 1993; Long *et al*. 1998). The neutron-diffraction data confirmed these measurements and are consistent with a random packing model, as observed for many thin amorphous metal films. The magnetic properties fall close to those of liquid iron.

In passing, we note that sonochemical techniques can also be used to prepare nanostructured alloys. For example, Fe–Co alloys have been synthesized from the readily available $Fe(CO)_5$ and $Co(CO)_3(NO)$ precursors. The composition of the Fe–Co alloys can be controlled simply by changing the ratio of solution concentrations of the precursors; alloy compositions ranging from pure Fe to pure Co are easily obtained (Hyeon *et al*. 1995).

(*b*) *Transition-metal colloids*

The existence of aggregates of nanometre clusters in our sonochemically prepared materials suggests the possibility of trapping these particles before they aggregate.

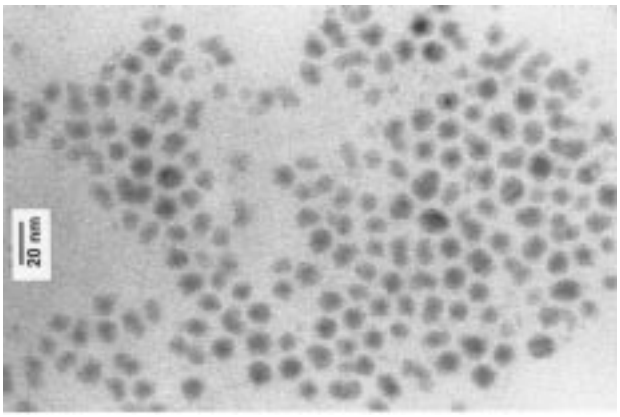

Figure 11. TEM of sonochemically prepared iron colloid stabilized by oleic acid (Suslick *et al*. 1996*a*).

Colloids of ferromagnetic materials are of special interest due to their many important technological applications as ferrofluids (Berkovsky *et al*. 1993). Such magnetic fluids find uses in information-storage media, magnetic refrigeration, audio reproduction and magnetic sealing. Commercial magnetic fluids are generally produced by exhaustive grinding of magnetite (Fe_3O_4) in ball or vibratory mills for several weeks in the presence of surfactants, which produces a very broad particle-size distribution.

We have developed a new method for the preparation of stable ferromagnetic colloids of iron. High-intensity ultrasound is used to sonochemically decompose volatile organometallic compounds in the presence of a colloid-stabilizing ligand (Suslick *et al*. 1996*a*). These colloids have narrow size distributions centred at a few nanometres and are found to be superparamagnetic. Sonochemical decomposition of iron pentacarbonyl in the presence of stabilizers such as polyvinylpyrrolidone or oleic acid produced a colloid of nanometre-sized iron particles. TEMs show that the iron particles have a relatively narrow range in size from 3 to 8 nm for polyvinylpyrrolidone, while oleic acid gives an even more uniform distribution at 8 nm (figure 11). Electron microdiffraction revealed that the particles are amorphous on the nanometre scale as formed and that during *in situ* electron-beam heating these particles crystallize to BCC iron.

Magnetic studies indicate that these colloidal iron particles are superparamagnetic with a respectable saturation magnetization of 101 emu g^{-1} (Fe) at 290 K. High-saturation magnetization is desirable for magnetic fluid applications and is highly sensitive to the method of preparation. Bulk amorphous Fe saturates at 156 emu g^{-1} (Fe) (Grinstaff *et al*. 1993; Bellissent *et al*. 1993). In comparison, the saturation magnetization of a commercial magnetite-based magnetic fluid is 123 emu g^{-1} (Fe) (Ferrofluids Corp. cat. no. APG-047).

(*c*) *Nanostructured molybdenum sulphide*

Very recently, we have reported the sonochemical synthesis of nanostructured molybdenum sulphide (Mdleleni *et al*. 1998). MoS_2 is best known as a standard automotive lubricant; its lubricant properties are due to its layered structure. Planes

of molybdenum atoms are sandwiched on both faces by planes of sulphur atoms tightly bonded to the Mo. Interactions between the sulphur planes are weak, thus producing lubrication properties similar to graphite. Of greater interest here, however, MoS_2 is also the predominant hydrodesulphurization catalyst, heavily used by the petroleum industry to remove sulphur from fossil fuels before combustion (Gates 1992).

We prepared an unusual morphology of MoS_2 by irradiating solutions of molybdenum hexacarbonyl and sulphur in 1,2,3,5-tetramethylbenzene with high-intensity ultrasound (Mdleleni *et al*. 1998). The MoS_2 was amorphous as initially prepared, but subsequently crystallized upon heating at 725 K for 10 h under an atmosphere of flowing He. EDX analysis performed on these particles gave a S to Mo atomic ratio of 2.06, identical within experimental error to bulk chemical analysis. The morphologies of the sonochemical and conventional MoS_2, however, are dramatically different, as shown in figure 12. Conventional MoS_2 shows a plate-like morphology typical for such layered materials. The sonochemical MoS_2 exists as a porous agglomeration of clusters of spherical particles with an average diameter of 15 nm.

Despite the morphological difference between the sonochemical and conventional MoS_2, TEM images of both sulphides show lattice fringes with interlayer spacings of 0.62 ± 0.01 nm. The sonochemically prepared MoS_2, however, shows much greater edge and defect content, as the layers must bend, break or otherwise distort to form the outer surface of the 15 nm particle size.

It is well established that the activity of MoS_2 is localized at the edges and not on the flat basal planes (Gates 1992; Pecoraro & Chianelli 1981). Unfortunately, most synthetic techniques yield a structure whose surface area is dominated by the basal planes. Given the inherently higher edge concentrations in nanostructured materials, the catalytic properties of our sonochemically prepared MoS_2 become especially interesting. To this end, the catalytic activity and selectivity for thiophene hydrodesulphurization (HDS) by sonochemically prepared MoS_2 was examined in a single-pass microreactor. Conventional MoS_2, sonochemical Mo_2C, commercial ReS_2 (Gallard–Schlesinger Ind., Carle Place, NY) and RuS_2 (Gallard–Schlesinger) were also investigated under the same conditions for purposes of comparison. For conventionally prepared sulphides, ReS_2 and RuS_2 are inherently more reactive than MoS_2 (Pecoraro & Chianelli 1981), but are too expensive to be generally used. Given the difference in edge versus basal surface activity, catalytic activity does not correlate with total surface area and therefore comparisons must be made on a catalyst mass basis.

The observed turnover frequencies as a function of temperature were measured for these catalysts using a standard solid–gas catalytic flow microreactor (Mdleleni *et al*. 1998). The principal products detected by GC were the C_4 hydrocarbons: butadiene, 1-butene, *trans*-2-butene, *cis*-2-butene and butane. No partially hydrogenated thiophenes were detected, and lighter (C_1–C_3) hydrocarbons accounted for less than 1% of the reaction products. The observed HDS activity order is

$$MoS_2 \text{ (sonochemical)} > RuS_2 \text{ (conventional)} > ReS_2 \text{ (conventional)} \sim Mo_2C \text{ (sonochemical)} > MoS_2 \text{ (conventional)}.$$

The sonochemically prepared MoS_2 catalyses the HDS of thiophene with activities roughly five-fold better than conventional MoS_2 and comparable to those observed with RuS_2, one of the best prior catalysts.

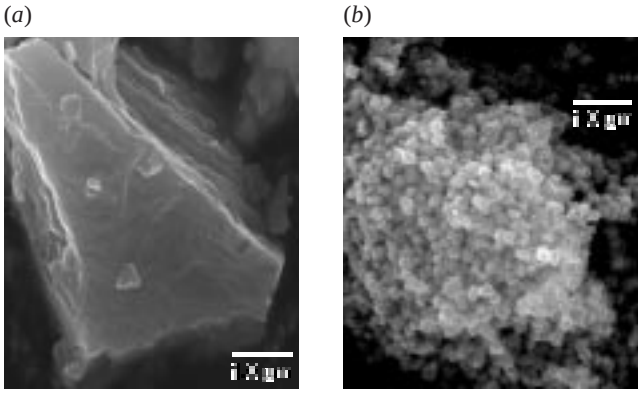

Figure 12. Morphology of (*a*) conventional and (*b*) sonochemically prepared MoS_2 (Mdleleni *et al*. 1998).

The product selectivities, expressed as percent of total C_4 hydrocarbons, observed at 375 °C were also examined. All catalysts showed high selectivity for formation of butenes, with the exception of the sonochemical MoS_2 that produced more butane. The accepted mechanism for thiophene HDS involves initial hydrogenolysis of the C–S bonds to give butadiene, followed by rapid hydrogenation to 1-butene, which is subsequently hydrogenated to butane or isomerized to a thermodynamic mixture of *cis*- and *trans*-2-butenes (Gates 1992). It is not surprising to see increased butane production from the sonochemical MoS_2, given its higher HDS activity.

There remains much to explore in the sonochemical synthesis of inorganic materials, and this technique has only begun to be exploited. The use of ultrasound in the synthesis of metal oxides, for example, has some promise as well (Shafi *et al*. 1997; Cao *et al*. 1997).

5. Sonochemical synthesis of biomaterials

Another important application of sonochemistry to materials chemistry has been in the preparation of biomaterials, most notably protein microspheres (Suslick & Grinstaff 1990; Liu *et al*. 1994; Wong & Suslick 1995; Eckburg *et al*. 1996; Webb *et al*. 1996). While the chemical effects of ultrasound on aqueous solutions have been studied for many years, the development of aqueous sonochemistry for biomaterials synthesis is very recent, particularly in the area of microencapsulation. It is beyond the scope of this article to review this area thoroughly, but a brief synopsis and bibliography will be provided.

Using high-intensity ultrasound and simple protein solutions, a remarkably easy method to make both air-filled microbubbles and non-aqueous liquid-filled microcapsules has been developed. Figure 13 shows an electron micrograph of sonochemically prepared microspheres. These microspheres are stable for months and, being slightly smaller than erythrocytes, can be intravenously injected to pass unimpeded through the circulatory system.

The mechanism responsible for microsphere formation is a combination of *two* acoustic phenomena: emulsification and cavitation. Ultrasonic emulsification creates the microscopic dispersion of the protein solution necessary to form the proteinaceous microspheres. Emulsification alone, however, is insufficient to produce long-

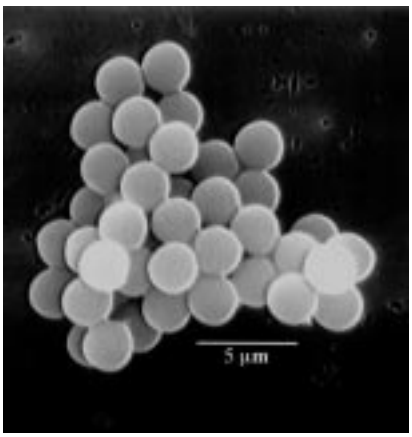

Figure 13. SEM of sonochemically prepared protein microspheres made from haemoglobin (Suslick 1998).

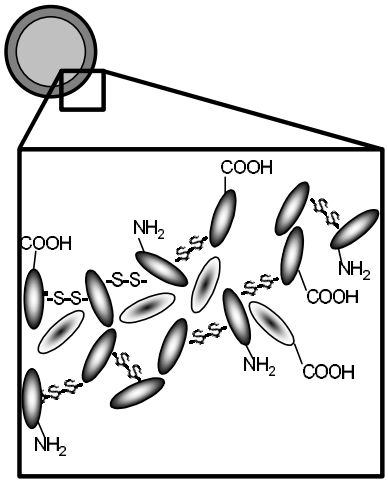

Figure 14. Disulphide cross-linking holds the protein microspheres together.

lived microspheres. The long life of these microspheres comes from a sonochemical cross-linking of the protein shell. Chemical reactions requiring O_2 are critical in forming the microspheres. It has been known for some time that the primary products from the sonolysis of water are H_2 and H_2O_2 coming $H^{\bullet}$ and $OH^{\bullet}$; in the presence of O_2, HO_2 is also produced (Riesz *et al*. 1985). We have used chemical trapping experiments to establish that the proteinaceous microspheres are held together by disulphide bonds between protein cysteine residues and that superoxide is the cross-linking agent. This is shown schematically in figure 14. The cross-linked shell of the microspheres is only about ten protein molecules thick, as shown in figure 15.

These protein microspheres have a wide range of biomedical applications, including their use as echo contrast agents for sonography (Keller & Feinstein 1988), as magnetic resonance imaging contrast agents (Liu *et al*. 1994; Eckburg *et al*. 1996; Webb *et al*. 1996), and for oxygen or drug delivery (Liu *et al*. 1994; Wong & Suslick 1995), among others. An extensive patent literature now exists in this area.

Figure 15. TEM of protein-stained microtome section from sonochemically prepared protein microspheres (Wong & Suslick 1995).

6. Conclusions

The chemical consequences of acoustic cavitation are far reaching. Bubble collapse in liquids creates unique high-energy conditions to drive chemical reactions in otherwise cold liquids. The utility of sonochemistry has been explored, and important applications have been developed for synthesis of unusual inorganic and biomedical materials.

This work was supported by the National Science Foundation and in part by the Department of Energy. We also thank M. Marshall, P. Mochel, V. Petrova and the UIUC Center for Microanalysis of Materials, which is supported by the Department of Energy, for their assistance in surface characterizations.

References

Barber, B. P. & Putterman, S. J. 1992 *Phys. Rev. Lett.* **69**, 3839.

Barber, P., Hiller, R., Arisaka, K., Fetterman, H. & Putterman, S. J. 1992 *J. Acoust. Soc. Am.* **91**, 3061.

Barber, P., Hiller, R. A., Lofstedt, R., Putterman, S. J. & Weninger, K. R. 1994 *Phys. Rev. Lett.* **72**, 1380.

Barber, B. P., Hiller, R. A., Loefstedt, R., Putterman, S. J. & Weninger, K. R. 1997 *Phys. Rep.* **281**, 65–143.

Bellissent, R., Galli, G., Grinstaff, M. W., Migliardo, P. & Suslick, K. S. 1993 *Phys. Rev.* B **48**, 15 797–15 800.

Berkovsky, B. M., Medvedev, V. F. & Krakov, M. S. 1993 *Magnetic fluids: engineering applications.* Oxford University Press.

Bernstein, L. S., Zakin, M. S., Flint, E. B. & Suslick, K. S. 1996 *J. Phys. Chem.* **100**, 6612–6619.

Cao, X., Prozorov, R., Koltypin, Y., Kataby, G., Felner, I. & Gedanken, A. 1997 *J. Mater. Res.* **12**, 402.

Cheeke, J. D. N. 1997 *Can. J. Phys.* **75**, 77–98.

Crum, L. A. 1994*a Phys. Today* **47**, 22.

Crum, L. A. 1994*b J. Acoust. Soc. Am.* **95**, 559.

Didenko, Y. T. & Pugach, S. P. 1994 *Ultrasonics Sonochem.* **1**, s10–s12.

Didenko, Y. T., Nastich, D. N., Pugach, S. P., Polovinka, Y. A. & Kvochka, V. I. 1994 *Ultrasonics* **32**, 71–76.

Doktycz, S. J. & Suslick, K. S. 1990 *Science* **247**, 1067.

Eckburg, J. J., Chato, J. C., Liu, K. J., Grinstaff, M. W., Swartz, H. M., Suslick, K. S. & Auteri, F. P. 1996 *J. Biomech. Engng* **118**, 193–200.

Flint, E. B. & Suslick, K. S. 1989 *J. Am. Chem. Soc.* **111**, 6987.

Flint, E. B. & Suslick, K. S. 1991*a* *J. Phys. Chem.* **95**, 1484.

Flint, E. B. & Suslick, K. S. 1991*b* *Science* **253**, 1397.

Flynn, H. G. 1964 Physics of acoustic cavitation in liquids. In *Physical acoustics* (ed. W. P. Mason), vol. IB, p. 157. New York: Academic.

Frenzel, H. & Schultes, H. 1934 *Z. Phys. Chem.* **27b**, 421.

Gates, B. C. 1992 *Catalytic chemistry*, pp. 387–392. New York: Wiley.

Gompf, B., Günther, R., Nick, G., Pecha, R. & Eisenmenger, W. 1997 *Phys. Rev. Lett.* **79**, 1405.

Grinstaff, M. W., Salamon, M. B. & Suslick, K. S. 1993 *Phys. Rev.* B **48**, 269.

Henglein, A. 1993 *Adv. Sonochem.* **3**, 17.

Hiller, R. A., Putterman, S. & Weninger, K. 1998 *Phys. Rev. Lett.* **80**, 1090.

Hyeon, T., Fang, M., Cichowlas, A. A. & Suslick, K. S. 1995 *Mater. Sci. Engng* A **204**, 186–192.

Hyeon, T., Fang, M. & Suslick, K. S. 1996 *J. Am. Chem. Soc.* **118**, 5492–5493.

Jeffries, J. B., Copeland, R. A., Flint, E. B. & Suslick, K. S. 1992 *Science* **256**, 248.

Keller, M. W. & Feinstein, S. B. 1988 In *Echocardiography in coronary artery disease* (ed. R. E. Kerber). New York: Future.

Leighton, T. G. 1994 *The acoustic bubble*, pp. 531–551. London: Academic.

Liu, K. J., Grinstaff, M. W., Jiang, J., Suslick, K. S., Swartz, H. M. & Wang, W. 1994 *Biophys. J.* **67**, 896–901.

Lohse, D., Brenner, M. P., Dupont, T. F., Hilgenfeldt, S. & Johnston, B. 1997 *Phys. Rev. Lett.* **78**, 1359–1362.

Long, G. J., Hautot, D., Pankhurst, Q. A., Vandormael, D., Grandjean, F., Gaspard, J. P., Briois V., Hyeon, T. & Suslick, K. S. 1998 *Phys. Rev.* B **57**, 10 716–10 722.

Mason, T. J. & Lorimer, J. P. 1988 *Sonochemistry: theory, applications and uses of ultrasound in chemistry*. Chichester, UK: Ellis Horword.

Mason, T. J. & Luche, J.-L. 1996 Ultrasound as a new tool for synthetic chemists. In *Chemistry under extreme or non-classical conditions* (ed. R. Van Eldik & C. D. Hubbard), pp. 317–380. New York: John Wiley.

Matula, T. J., Roy, R. A., Mourad, P. D., McNamara III, W. B. & Suslick, K. S. 1995 *Phys. Rev. Lett.* **75**, 2602.

Mdleleni, M. M., Hyeon, T. & Suslick, K. S. 1998 *J. Am. Chem. Soc.* **120**, 6189–6190.

Moser, W. R. (ed.) 1996 *Advanced catalysts and nanostructured materials*. New York: Academic.

Moss, W. C., Clarke, D. B. & Young, D. A. 1997 *Science* **276**, 1398–1401.

Neppiras, E. A. 1980 *Phys. Rep.* **61**, 159–251.

Pecoraro, T. A. & Chianelli, R. R. 1981 *J. Catal.* **67**, 430.

Preece, C. M. & Hansson, I. L. 1981 *Adv. Mech. Phys. Surf.* **1**, 199.

Putterman, S. J. 1995 *Scient. Am.* (Febraury), p. 46.

Rayleigh, Lord 1917 *Phil. Mag.* **34**, 94.

Richards, W. T. & Loomis, A. L. 1927 *J. Am. Chem. Soc.* **49**, 3086.

Riesz, P., Berdahl, D. & Christman, C. L. 1985 *Environ. Health Perspect.* **64**, 233.

Shafi, K. V. P. M., Gedanken, A., Goldfarb, R. B. & Felner, I. 1997 *J. Appl. Phys.* **81**, 6901.

Suslick, K. S. (ed.) 1988 *Ultrasound: its chemical, physical, and biological effects*. New York: VCH.

Suslick, K. S. 1990 *Science* **247**, 1439.

Suslick, K. S. 1994 Sonochemistry of transition metal compounds. In *Encyclopedia of inorganic chemistry* (ed. R. B. King), vol. 7, pp. 3890–3905. New York: John Wiley.

Suslick, K. S. 1995 *MRS Bull.* **20**, 29.

Suslick, K. S. 1997 Sonocatalysis. In *Handbook of heterogeneous catalysis* (ed. G. Ertl, H. Knozinger & J. Weitkamp), vol. 3, ch. 8.6, pp. 1350–1357. Weinheim: Wiley-VCH.

Suslick, K. S. 1998 Sonochemistry. In *Kirk–Othmer encyclopedia of chemical technology*, 4th edn, vol. 26, 517–541. New York: John Wiley.

Suslick, K. S. & Crum, L. A. 1997 Sonochemistry and sonoluminescence. In *Encyclopedia of acoustics* (ed. M. J. Crocker), vol. 1, ch. 26, pp. 271–282. New York: Wiley-Interscience.

Suslick, K. S. & Doktycz, S. J. 1990 The effects of ultrasound on solids. In *Advances in sonochemistry* (ed. T. J. Mason), pp. 197–230. New York: JAI.

Suslick, K. S. & Grinstaff, M. W. 1990 *J. Am. Chem. Soc.* **112**, 7807.

Suslick, K. S., Hammerton, D. A. & Cline Jr, R. E. 1986 *J. Am. Chem. Soc.* **108**, 5641.

Suslick, K. S., Choe, S. B., Cichowlas, A. A. & Grinstaff, M. W. 1991 *Nature* **353**, 414.

Suslick, K. S., Flint, E. B., Grinstaff, M. W. & Kemper, K. A. 1993 *J. Phys. Chem.* **97**, 3098–3099.

Suslick, K. S., Fang, M. & Hyeon, T. 1996*a* *J. Am. Chem. Soc.* **118**, 11 960–11 961.

Suslick, K. S., Hyeon, T. & Fang, M. 1996*b* *Chem. Mater.* **8**, 2172–2179.

Webb, A. G., Wong, M., Kolbeck, K. J., Magin, R. L., Wilmes, L. J. & Suslick, K. S. 1996 *J. Mag. Res. Imaging* **6**, 675–683.

Weller, H. 1993 *Adv. Mater.* **5**, 88.

Wong, M. & Suslick, K. S. 1995 Sonochemically produced hemoglobin microbubbles, hollow and solid spheres and microspheres. In *MRS Symp. Proc.* (ed. D. L. Wilcox, M. Berg, T. Bernat, D. Kellerman & J. K. Corchran), vol. 372, pp. 89–94. Pittsburgh, PA: Materials Research Society.